UNITVERSITY OF CALIFORNIA

Los Angeles

Electronically-Tunable Resonant Blazed Metasurface Grating

A thesis submitted in partial satisfaction

of the requirements for the degree

Master of Science in Electrical Engineering

by

Haozhan Tian

2017

ABSTRACT OF THE THESIS

Electronically-Tunable Resonant Blazed Metasurface Grating

by

Haozhan Tian

Master of Science in Electrical Engineering

University of California, Los Angeles, 2017

Professor Tatsuo Itoh, Chair

Blazed gratings have so far been made tunable by mechanically changing the grating geometry, such as its periodicity. In this work, a low-profile planar blazed metasurface grating is demonstrated which is electronically tunable, with no moving or mechanically changing parts. The reflective metasurface is comprised of planar patch resonators with a cutting slot loaded with a surface mount varactor in each unit cell, and is demonstrated numerically and experimentally in Part 1. Coupling of the incident wave to the resonant surface provides a high efficiency back reflection or blazing. We show that by changing the DC bias, we are able to control the strip resonance, which in turn controls the Bragg blazing frequency and the reflection angle of the operation. This tuning has been confirmed by simulations and measurements for the Transverse Magnetic polarized incident wave within the X-band. In Part 2, several design are proposed to overcome the problems of the original design and improve

the performance. The ground-slotted design, which maintains a simple strip resonator and places the bias on the ground plane, appears to achieve strong blazing using fewer varactors. Meanwhile, the separated bias system for ground-slotted design helps to identify defective varactors during fabrication. Future work is proposed in the final section to further refine the design and have a promised measurement result.

The thesis of Haozhan Tian is approved.

Benjamin S. Williams

Mona Jarrahi

Tatsuo Itoh, Committee Chair

University of California, Los Angeles

2017

To my beloved families.

TABLE OF CONTENTS

TABLE OF FIGURES

ACKNOWLEDGEMENT

First, I would like to express my sincere gratitude to Professor Tatsuo Itoh for his generous help for my master's study. It was him who support me to do the research I want and showed me how to be a good researcher.

Second, I would like to thank Doctor Mohammad Memarian for his direct guidance in my project. His knowledge and experiences greatly helped me in the project.

Third, I would also like to thank Cheng Tao, Kirti Dwaj, Xiaoqiang Li. They warmly welcome me to the lab and gave me a lot of help. I am so lucky to join in the lab and work with them. Meanwhile, I would like to thank all the friends here in UCLA. Their company made my life colorful.

In the end, I would like to greatly thank my parents and my wife. Nothing would happen without their unconditional support.

Part 1

Tunable Blazed Gratings with a Single Split Patch in the Unit Cell

1.1 Introduction

A typical diffraction grating is a periodic structure which will scatter the incident wave into different directions, also known as diffracted orders. It has been widely used in optics to split the lights with different frequencies. Depending on the periodicity, a grating can have several diffracted orders (directions) for an incident wave with certain frequency.

As one type of the diffraction gratings, blazed diffraction gratings can scatter an oblique incident wave into a certain direction (the $m = -1$ diffraction order) with low or even zero specular ($m = 0$) reflection. The $m = -1$ diffracted order can be in the same angle as the incident wave (auto-collimation). Typical blazed gratings such as sawtooth grating [1] or groove gratings [2] are widely used non-planar gratings for different applications in microwaves and optics, e.g. Littrow cavities and lasers. In Littrow mount cavities, mechanical rotation of the grating can tune the laser frequency, since the auto-collimation frequency and incident angles are related.

Recently, low-profile blazed grating designs using metasurfaces (MSs) and equivalent resonant structures have been reported in [3-5]. MSs are practically very thin structures engineered for controlling phase and magnitude of local wave, and can be used to shape the scattered wave-front. The reported planar blazed gratings are achieved either by phase-modulated metasurfaces [3], or by resonant element(s) e.g. resonant strip(s) in the unit-cell [4, 5], as shown in Figure 1 (a). Besides its simple design and strong blazing performance, the

resonant blazed MS grating of [4, 5] have a unique fundamental operation that opens a door to further tailor the blazing operation.

Tunable metasurfaces [6-15], offering the way to further tailor the operation of a subwavelength structure, have been studied recently. Based on the tuning purposes, these metasurfaces can be categorized into intensity modulator, phase modulator, polarization modulator, and frequency tuning. Based on the tuning methods, these can be generally categorized into electronical tuning, mechanical tuning, optical tuning, and thermal tuning. In all these tunable metasurfaces, frequency tuning metasurface is what we are interested in here. It has to be mentioned that besides the four main methods, there are still other ways to achieve frequency tuning, such as using liquid metal, piezoelectric actuator to change the size of the resonant cavity, elastic substrate to tune the frequency by stretching the structure, and also graphene due to its amazing tunability. In general, electronically tunable metasurfaces are desired because as it is easier to apply electrical bias and is relatively more reliable compared with other methods.

Tunable blazed gratings have been reported in the past by mechanically changing the grating as in [6]. Thus they required some form of mechanical movement or actuation (e.g. MEMS), which can make them quite challenging to fabricate and operate. In this work, we design and demonstrate an electronically tunable resonant blazed MS grating with no moving parts, to control the blazing frequency and scattering angle of operation, with its principle depicted in Figure 1 (b). We utilize a fixed period resonant grating similar to [4, 5], but tune the internal resonance in each period using surface mount varactor (SMV), achieving a tunable

blazed surface. Bi-static radar measurements with fixed incident angle show that the scattered wave scans as the bias changes. Such a design can find various applications, including Littrow setups where the gratings is no longer needed to be moved, and the output frequency can still be tuned.

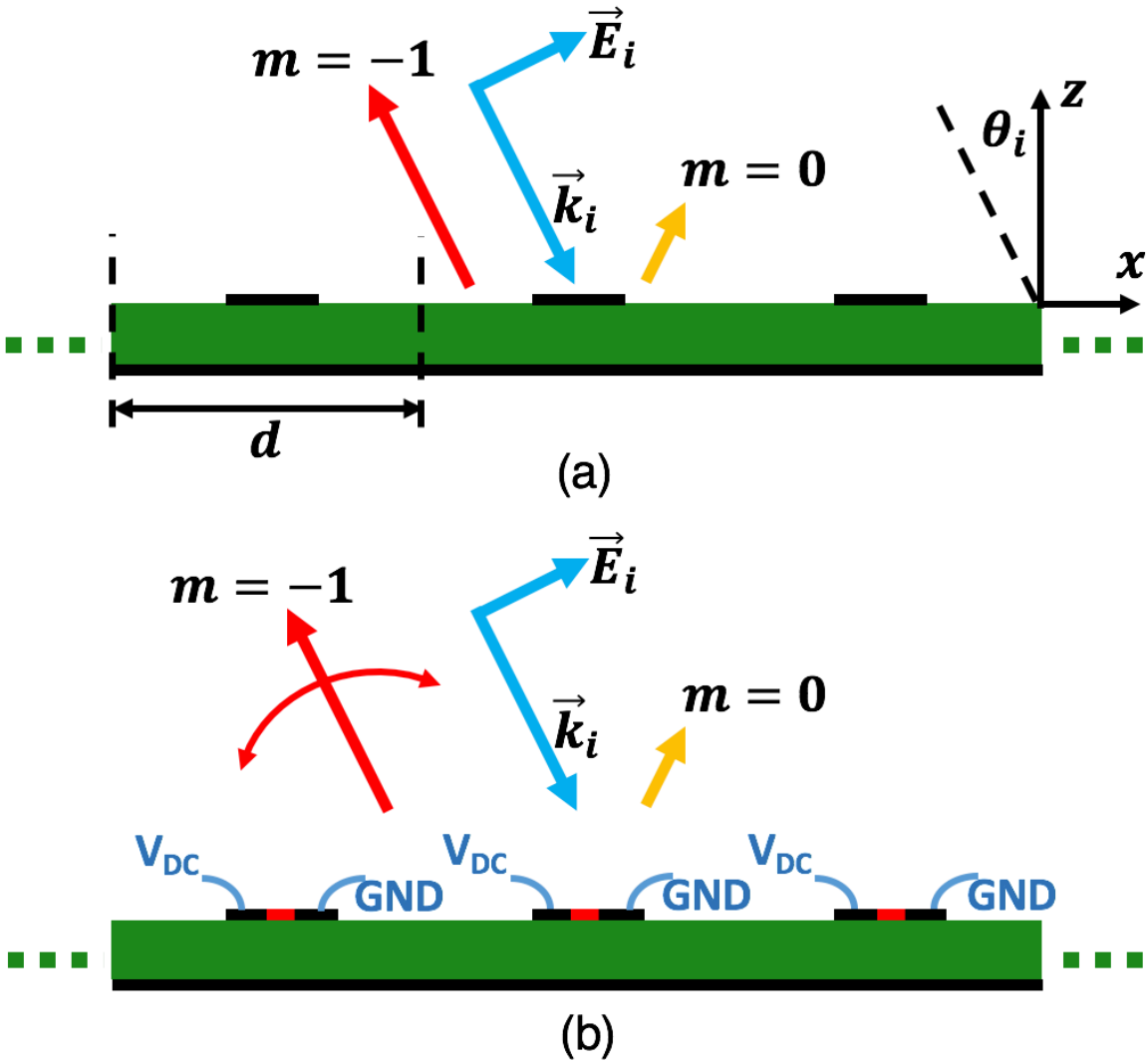

Figure 1 (a) Resonant blazed MS grating [4, 5] infinitely periodic in *x* direction with period *d* under Transverse Magnetic (TM) polarized incident wave, with strong *m = –1* and low specular *m = 0* scatter. (b) Electronically-tunable resonant blazed grating with DC-bias SMVs (represented by the red bars).

1.1.1 Grating Equation and Bragg Condition

The frequency of the oblique incident wave determines the diffraction angle of space harmonics for a constant incident angle and fixed period of the grating. The grating equation

for propagating waves in vacuum relates periodicity of the structure (d), the diffraction order (m), the operating wavelength (λ_0), angle of incidence (θ_i), and the angle of the diffracted order (θ_m) by:

$$\sin\theta_i + \sin\theta_m = \frac{m\lambda_0}{d} \tag{1}$$

Thus for a grating with fixed period d and incident angle θ_i, the angle of diffracted $m = -1$ wave θ_{-1} scans as the frequency of the incident wave changes. An efficient blazed grating scatters most of the power to the $m = -1$ wave and with minimal specular $m = 0$ wave.

For auto-collimation, the incident and diffracted $m = -1$ wave angles are identical, which means the grating can reflect the incident wave back along the path of the incidence depending on the amount of specular reflection ($m = 0$ diffracted wave). To achieve auto-collimation, the Bragg condition needs to be satisfied [5]:

$$k_0 d \sin\theta_i = \pi \tag{2}$$

Confined by this condition, a grating with a fixed period can only achieve auto-collimation blazing at a particular frequency when shined with the specific Bragg incident angle.

1.1.2 Tunable Resonant Blazed MS Grating

The operation theory of resonant MS grating [4, 5] is that the incident wave couples to the low order resonance of each strip resonator in each cell, at the point of strong blazing. Underneath the strip, the transverse resonant mode is excited. The two ends of the strips that have two E-field maxima with anti-parallel direction act like two in-phase magnetic currents.

In order to have the strongest coupling, the resonant frequency of the resonator has to be

the same as the frequency of the incident wave. The value of coupling has little to do with the periodicity of the whole structure, and depends on the geometry of the resonator inside the unit-cell. For a strip with a particular resonant frequency, the highest efficiency blazing point will be at an incident angle that Bragg condition (2) is satisfied, for that particular frequency and period. Thus, for a resonant MS grating with a constant period, the resonant frequency of the interior of the unit-cell determines the efficiency of the diffracted $m = -1$ wave for a given incident wave.

If the resonant frequency can be tuned, the frequency at which the maximum efficiency of diffracted $m = -1$ (and minimum specular) occurs also tunes. The frequency change causes the diffracted angle θ_{-1} to scan. The relation of the tuning frequency and the scanning angle is governed by (1) where all parameters are fixed except λ and θ_{-1}. If auto-collimation is desired, the incident angle must further depend on the resonant frequency satisfied by (2), in order to have strongest blazing on the Bragg line. We utilize tunable patch resonators, instead of fixed passive strips of [4, 5], to individually bias each unit-cell, and electronically tune the resonance frequency.

1.2 Design Guideline

In this work, all the designs are based on Rogers RT/duroid® 5880 Laminates substrate with dielectric constant of 2.2, a tangent loss of 0.0009 and a thickness of 1.57mm.

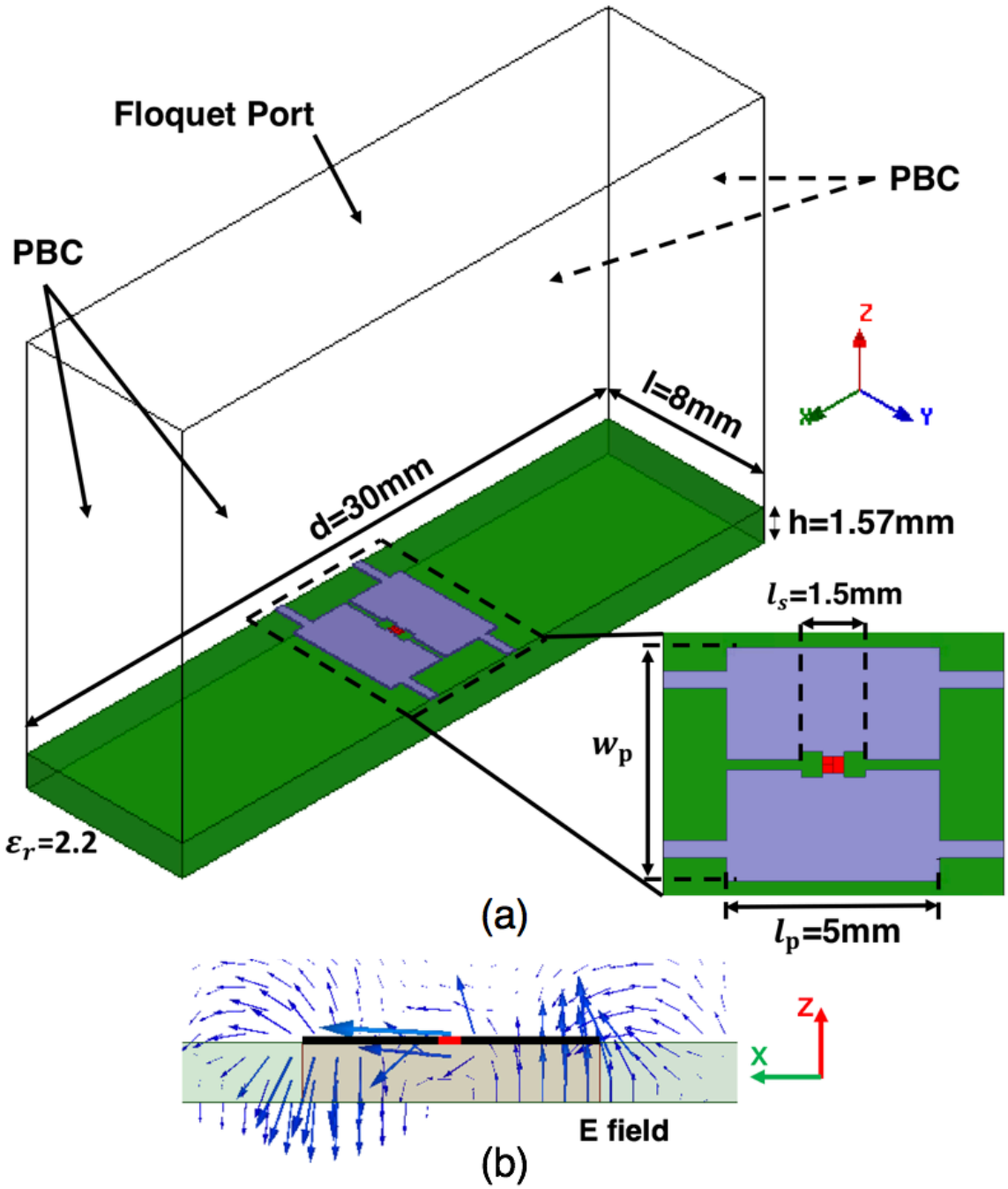

Figure 2 (a) Unit-cell of grating with a tunable patch, under oblique TM polarized incidence, optimized for auto-collimation at $\theta_i = \theta_{-1} = 30°$. (b) Electric field profile shows resonance under the tunable patch.

1.2.1 Tunable Split Patch Resonator

The unit cell of the grating is shown in Figure 2 (a). The period of the structure '*d*' is chosen as *30 mm* in order to satisfy the Bragg condition (2) in the X-band, and for blazing to occur in the *x-z* plane. The length of the unit cell '*l*' is *8 mm*. A grounded Rogers substrate

RT5880 is used for the structure due to its low loss. The 1.57-mm thick substrate has dielectric constant of 2.2, dielectric loss tangent of 0.0009, and 2-oz copper cladding whose conductivity is 5.8×10^7 S/m. The main structure of the unit cell is a tunable patch resonator, split by a cutting slot. The width of the patch w_p is 5.5 mm and the length l_p is 5 mm. It is intended to operate similarly as the strip of [4, 5] in a low order resonance in the x-direction.

This tunable patch resonator is inspired by Patch Antenna with Switchable Slots (PASS) [7]. It has been reported that the cutting slot on a patch antenna will affect the surface current flow and thus have an influence on the resonant frequency. The slot is typically loaded by a capacitor. Here the slot, with length l_s 1.5 mm, is placed in the middle as the current reaches maximum in the center of the patch, so that the slot can have the most significant effect on the resonant frequency [7]. The slot is supposed to be loaded by a SMV so that the capacitance can be tuned by the DC bias. Here in the design model, a red square, which is defined by Lumped RLC Boundary in Ansys HFSS, represents the varactor. For design simplicity, a capacitor is used initially for unit-cell simulation. For prototype design, the equivalent circuit model of the varactor given by the vendor is used to accurately simulate its behavior. In addition, a thin split is designed to block DC current for bias considerations. Since the split is very thin, it will not affect the RF current much. The thin strips at the end of the patch are the bias lines connecting all the patches. All biasing is done on the top metallization, and there is no need for ground access or vias.

The simulated electric field plot in Figure 2 (b) shows that the incident TM wave indeed couples to the transverse resonant mode of design, which is similar to that of the fixed resonant

strip of [4, 5]. The frequency of this resonant mode is now controlled by the varactor in the middle of the patch.

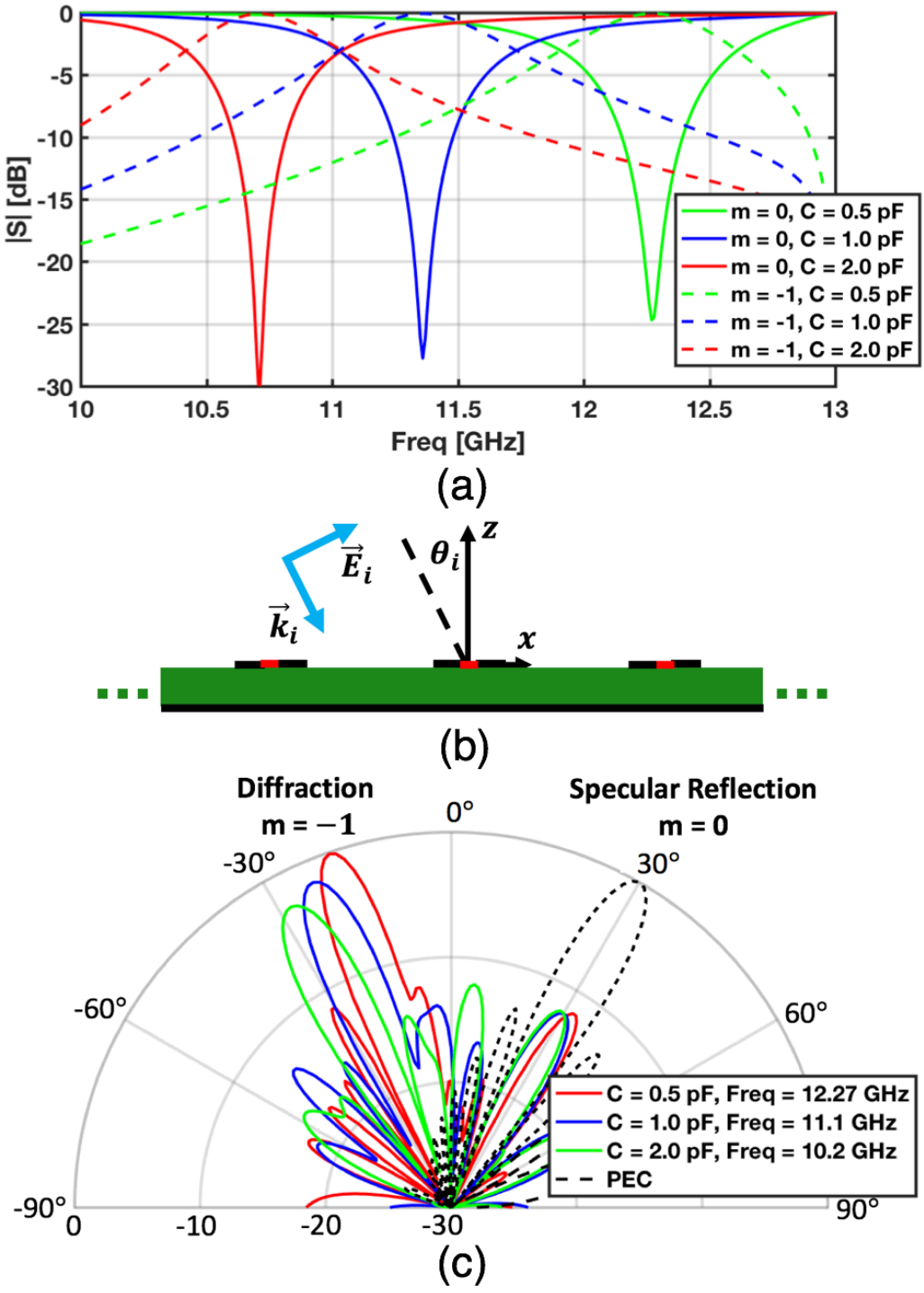

Figure 3 (a) Simulated magnitude of specular ($m = 0$) and $m = -1$ waves as a function of frequency at three different capacitances of the structure. (b) Structure under incident TM wave. (c) Simulated scattering (in dB) of a finite sample at resonant frequencies with θ_i = -30°. The patterns are normalized by max. reflection of a same size PEC at f = 12.27 GHz (black dash line).

1.2.2 Simulation Results

The structure shows frequency tuning for blazing operation when the varactor capacitance changes. The tuning can be seen in periodic unit-cell simulation results of Figure 3 (a), showing specular reflection ($m = 0$) and $m = -1$ diffraction vs. frequency, for a fixed incident angle $\theta_i = 30°$. The frequency of diffraction maxima is the same as the one of specular reflection minima, at which strong blazing appears. This indicates strong coupling between the incident wave and the resonator at these frequencies. Meanwhile, the resonant frequency increases as the capacitance decreases as we expected. The tuning frequency range of this unit cell design is slightly beyond X band (12 GHz). This is because the varactor is modeled by a capacitor here, while in reality the varactor has an additional package inductance which will offset the capacitance in some extent and decrease the tuning frequency.

The simulated scattering patterns of a finite sample for three different capacitances are given in Figure 3 (c). As the capacitance changes, the resonant frequency varies and the diffracted beam scans, which follows the grating equation (1). The result also shows that at the resonant frequencies, most of power is diffracted to $m = -1$ mode and the specular reflection is minimized. This simulation is aimed to prove the tunability of the finite size board and thus no loss or package inductance is considered. Due to the finite size, the resonant frequencies are slightly different from the ones given by the unit-cell simulation. Any fixed blazed grating under this fixed incident angle and period achieves its specular minima at a single frequency, however, with our design, we are tuning the strong blazing to other frequencies by changing the varactor capacitance.

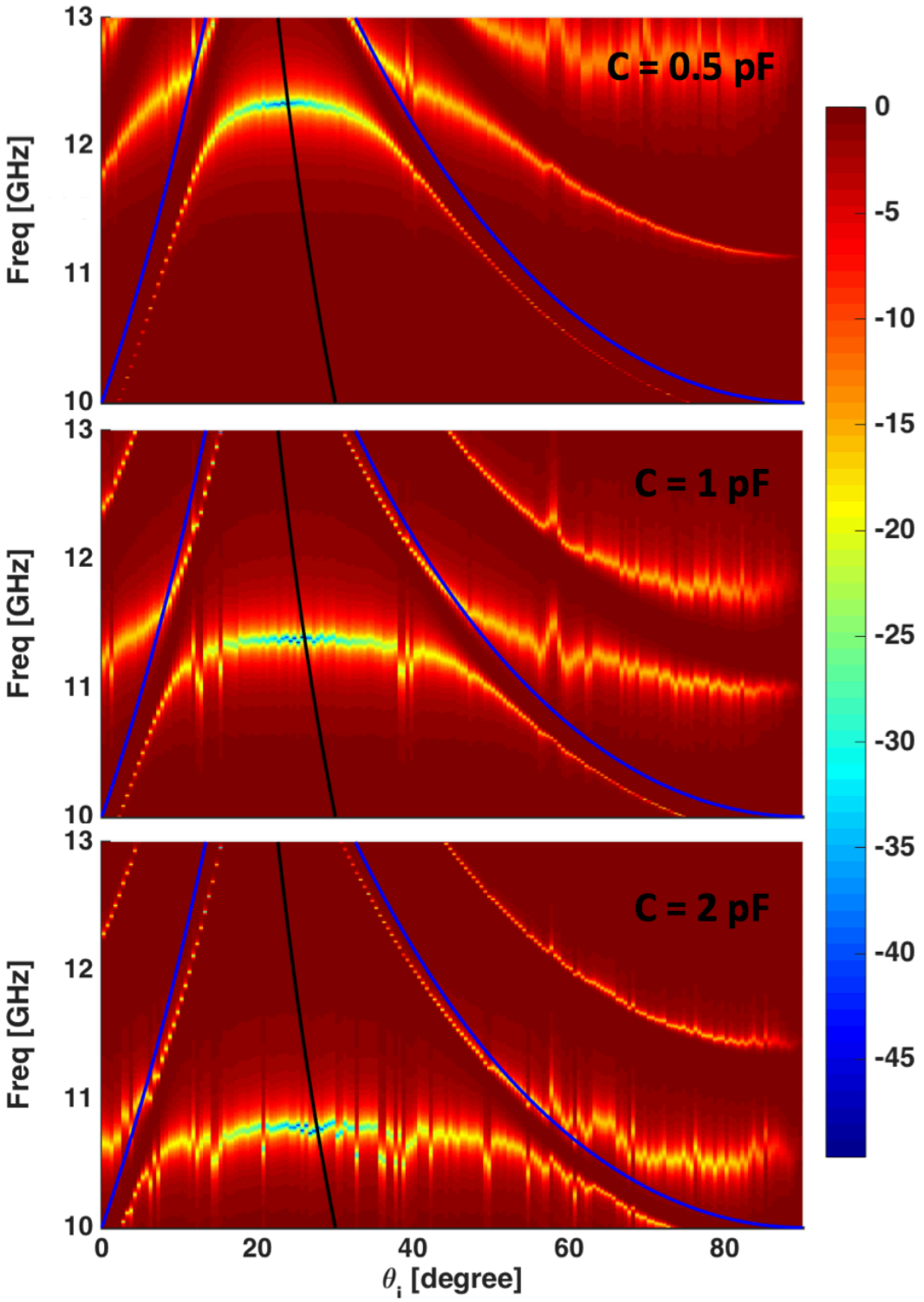

Figure 4 Specular reflection (dB) as a function of the operation frequency and incident angle. The black line shows the path of the Bragg condition. Between the blue lines are the operation regions, only supporting m = 0, –1 waves.

The tunability of the structure can also be verified under Bragg condition (2). Figure 4 shows the specular reflection as a function of frequency and incident angle of the same unit

cell at three different capacitances. The path of Bragg condition for $d = 30\ mm$ is shown by the black line. Lower specular reflection implies stronger blazing. It can be observed that as the capacitance increases, the frequency of the strongest blazing point (specular minima) decreases and this blazing point moves along Bragg line. Thus this grating design is able to achieve multiple auto-collimation blazing without changing the periodicity of the structure, at different varactor bias levels.

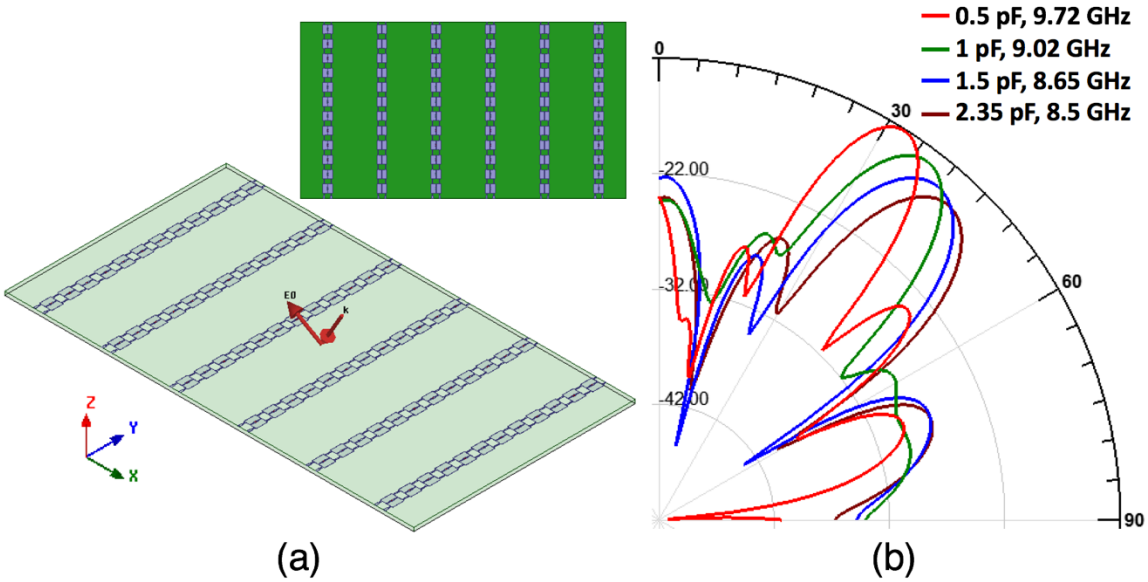

Figure 5 (a) A finite 6×12-cell sample. (b) Simulated scattering (in dB) at $\theta_i = 30°$ showing that when the capacitance is tuned, the frequency of maximum diffracted $m = -1$ wave will also be tuned, thus the diffracted angle θ_{-1} scans.

A finite sample containing 6×12 unit cells of such grating is simulated to show the scattering, as in Figure 5 (a). For this simulation, the varactor is modeled by equivalent circuit by Skyworks SMV 1231 varactor, the one used for fabrication. When the varactor capacitance changes, the frequency of maximum diffracted $m = -1$ wave is tuned, which causes the diffracted angle θ_{-1} to change, as shown in Figure 5 (b). Four different capacitances are used to show the tuning. The magnitudes of all the four diffractions are normalized to the strongest one at capacitance equal to 0.5 pF.

1.3 Measurement of the Prototype of Tunable Grating

A sample containing 6 by 12 unit cells was fabricated as shown in Figure 6. The bias line is attached at the end of each column. Since most RF current flows on the patch, and the thin bias lines barely transmit RF current, there is no need to design RF chokes at the end of bias lines. This has been verified by simulation. The varactor is pasted in the center of the patch by silver conductive epoxy which is claimed to have low loss at high frequency. The grounded Rogers RT5880 is used, same board as the one in simulation.

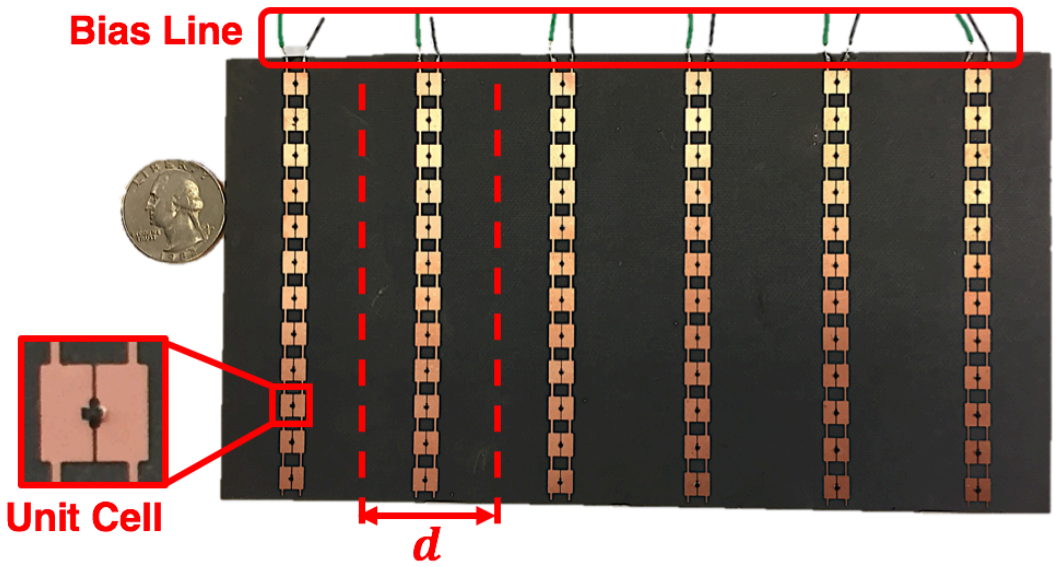

Figure 6 A finite 6×12-cell tunable resonant blazed grating prototype with periodicity $d = 30\ mm$.

1.3.1 Measurement Setup

Bi-static radar measurement settings are used, as shown in Figure 7. The tunable grating board is placed at the far-field region of both the transmitted and received antennas. The distance between the board and the two antennas are fixed. The received antenna is rotated to capture the diffraction field at different angles under different bias voltages. The DC source for biasing is placed behind the absorbers to avoid undesired scattering.

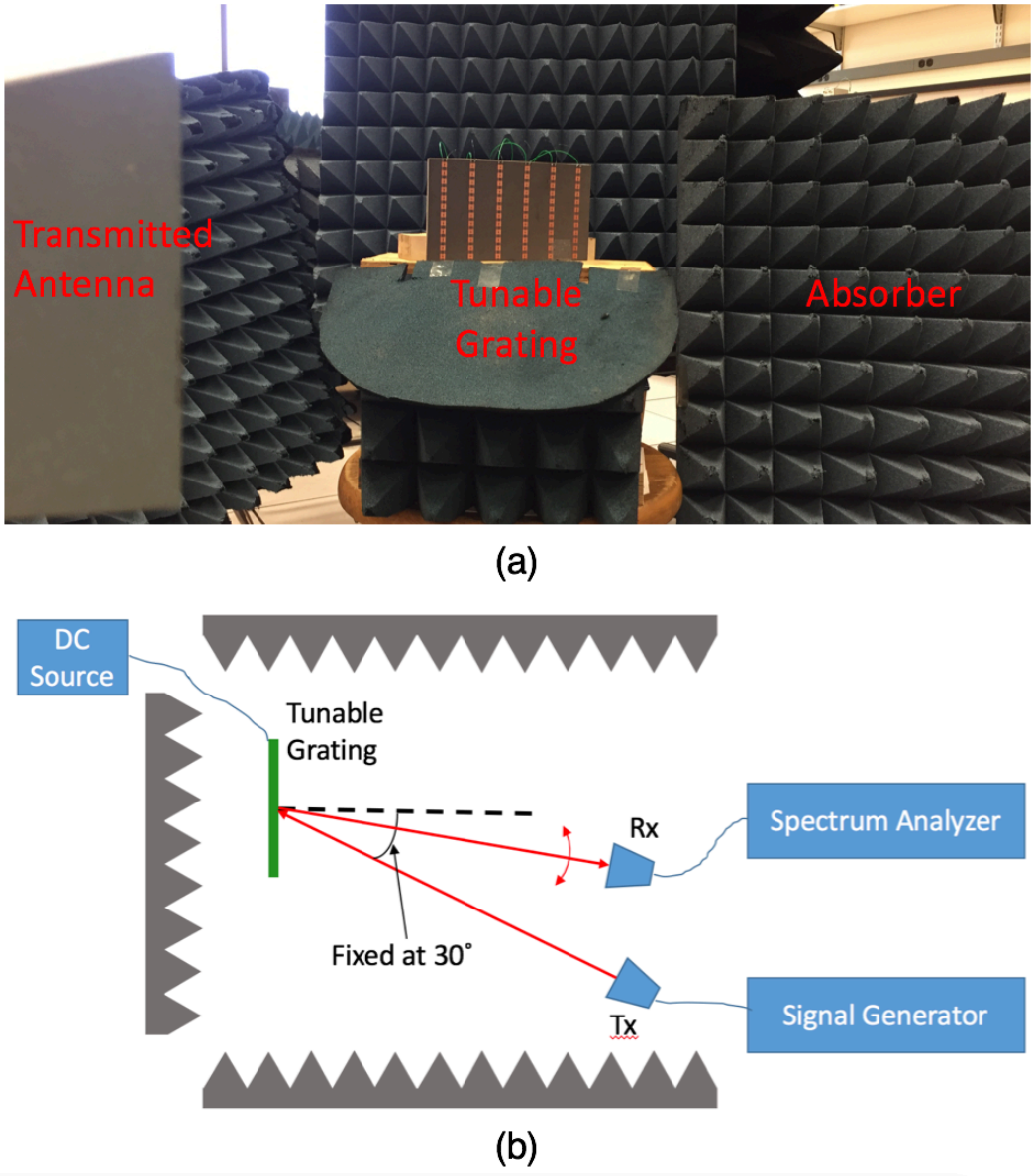

Figure 7 The measurement setup: (a) real measurement setups (b) scheme of the measurement setups

1.3.2 Scattering Pattern Measurements

Bi-static radar measurement results from the surface are shown in Figure 8. The transmitting antenna is set at $\theta_i = 30°$ at the far field region, and the receiving antenna scans to capture the diffracted $m = -1$ wave. The measurement is operated within X band. In order to improve the measurement accuracy, we process the data with time-grating method [18]. It basically selects the target data in time domain so that we can avoid the undesired scattering

from scatterers other than the grating sample. The results clearly indicate that a fixed grating, under a fixed incident angle, has a frequency scanning for the $m = -1$ back reflected beam as bias voltage is changed. The operating frequencies, calculated by (1) for the grating with same period and angle as the sample here, are shown by the dots in Fig. 8, which basically match the measured results. It has to be mentioned that higher the bias voltage is, lower the capacitance is for a hyperabrupt junction varator used here. Since we are only able to control the DC source for the bias, the capacitances shown in Figure 8 are translated from the data sheet given by the vendor.

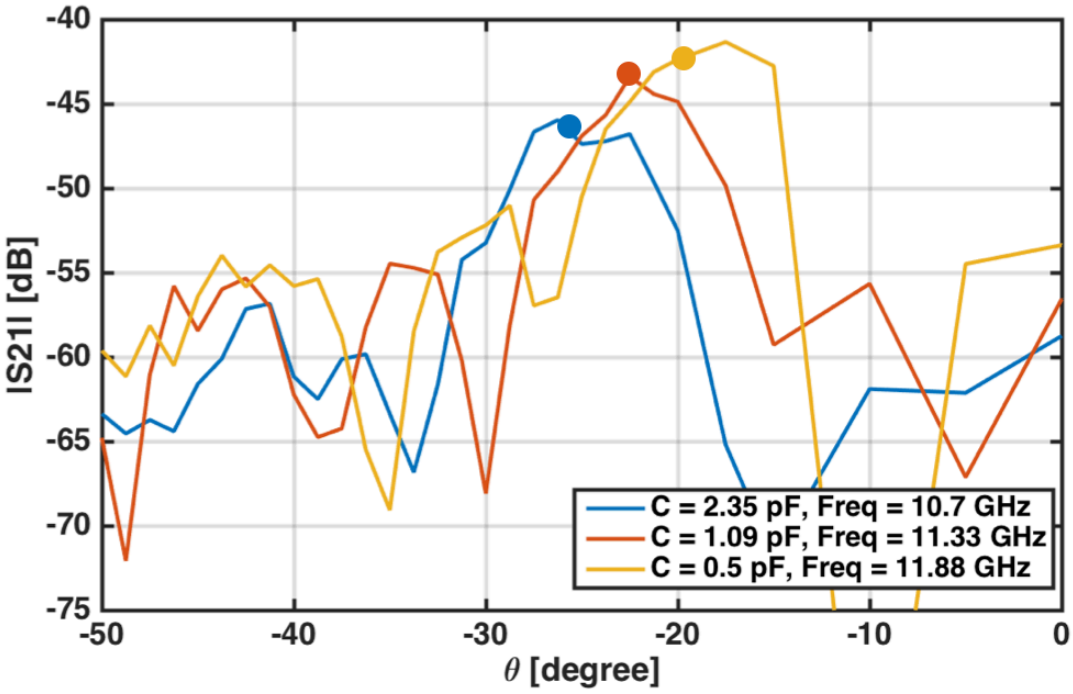

Figure 8 Measured scattering pattern at different capacitances (different bias voltages), causing the diffracted $m = -1$ wave peak to scans from 18° to 26° along with tuning the frequency of maximum scatter. The dots indicate the diffracted angles of $m = -1$ mode for the three operating frequencies at fixed $\theta_i = 30°$ which satisfy the grating equation (1).

1.4 Discussion

The measured scattering is relatively low. The blazing is weak indicating that the coupling

is weak for the fabricated sample. Compared with real structure, the model of the varactors in simulation are uniformly distributed 2D layers with equivalent circuit model given by the vendor which may not be accurate within the band we are dealing with here. This modeling method of varactor is relatively simple which may lead to an inaccurate simulation results. Another possible reason for the weak blazing is that the capacitances for the fabricated sample are not all uniformly distributed. This may be caused by: 1) Some of the varactors don't function well; 2) Some may not be well connected to the resonators; 3) Bias voltage may not be uniformly distributed over each varactor. For the 12 by 6 unit-cell sample, total of 72 varactors are used, which is a relatively large number. And in order to have a convenient bias, we shunt 12 varactors for each column, which means, except the very first varactor on each column, we are unable to test if the varactor functions well or is well connected to the patch after soldering.

To see if the non-uniform capacitances can cause the weak blazing, in simulations, we randomly remove one varactor of each column in the same 6 by 12 sample used before, as shown in Figure 9 (a). In this way, we try to mimic the possible situation of a fabricated sample that some of the varactors didn't function well. The simulation results are shown in Figure 9 (b), where the resonant frequencies for each capacitances are same as the one shown in Figure 5 (b). We can see that as the capacitance changes, the diffraction beam still scans as we expected; however, the blazing for all four capacitances is much weaker than the specular reflection when in total 6 varactors are open-circuit. The blazing is also much weaker than the one that all the varactors work well.

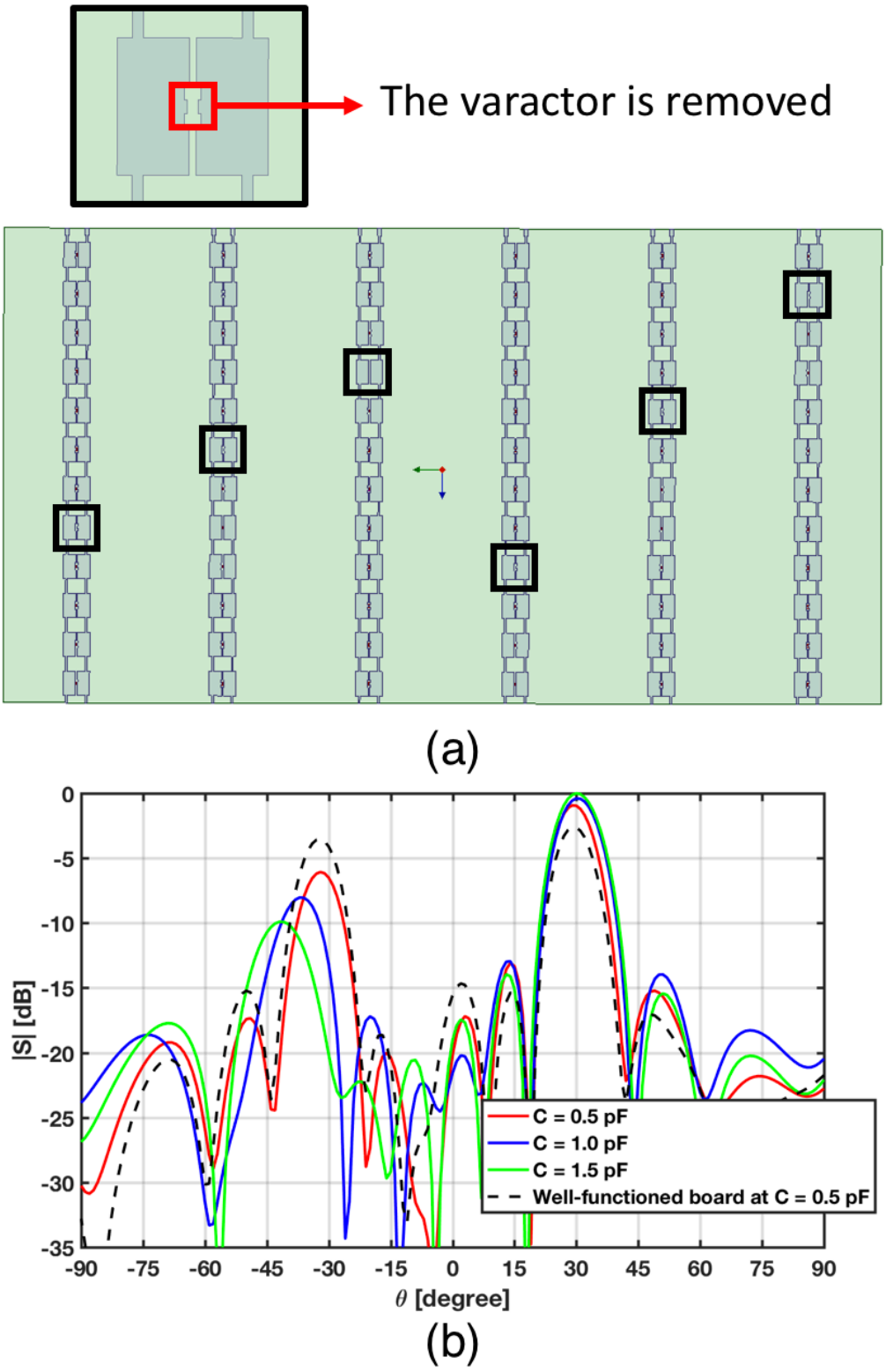

Figure 9 (a) A finite 6×12-cell sample with the varactors in the black boxes are removed (open-circuit). (b) Simulated scattering (in dB) at θ_i = 30° showing that the grating is still tunable but the magnitude of the diffracted field is much weaker than the one of specular reflection.

We measured the total capacitance for each column of the sample grating. It turns out that

each column doesn't share the same total capacitance. The highest capacitance is around 22 pF, while the lowest capacitance is around 16 pF. This indicates that there are several varactor that are not well-functioned. They are either not well connected or simply broken. The capacitance for SMV 1231 without bias is 2.35 pF. There are 12 varactors for each column in total. So the total capacitance without bias should be around 28 pF. However, the multimeter will apply certain voltage to the varactor in order to measure its capacitance. Since higher bias voltage leads to a lower capacitance, the total measured capacitance could be lower than 28 pF. So the non-uniform distribution of the capacitance of the sample can be the main reason for the weak blazing.

In addition, we also simulate the same sample with all the varactors removed. The result shows that there is only specular reflection with basically same magnitude as the one of a same size PEC. No backward blazing is detected in that simulation. The two simulations indicate that each of the varactors in this design is extremely important and we have to make sure they function well, in order to detect a strong blazing result as predicted by simulation. And thus we have to make sure they function well during fabrication before measuring.

Another main reason is that the loss of the varator we used for fabrication is too high. A better option is to use the abrupt junction varactor which needs higher tuning voltage but has lower loss than the hyperabrupt one. To prove that, a simulation of the same structure with varactors modeled by the equivalent circuit model of Skyworks SMV 1405 is run at $\theta_i = 30°$. The simulated blazing peak is around 4 dB higher than the one modeled by SMV 1231, and the reflection peak is around 4 dB lower than the one of SMV 1231, as shown in Figure 10. Due

to the different package inductances for the two models, the resonant frequencies for the same structure at the same total capacitance are different for the two simulations. And thus the angles of the diffraction peak are different. In conclusion, a higher-Q varactor, namely SMV 1405, will be applied in the next design to improve the performance.

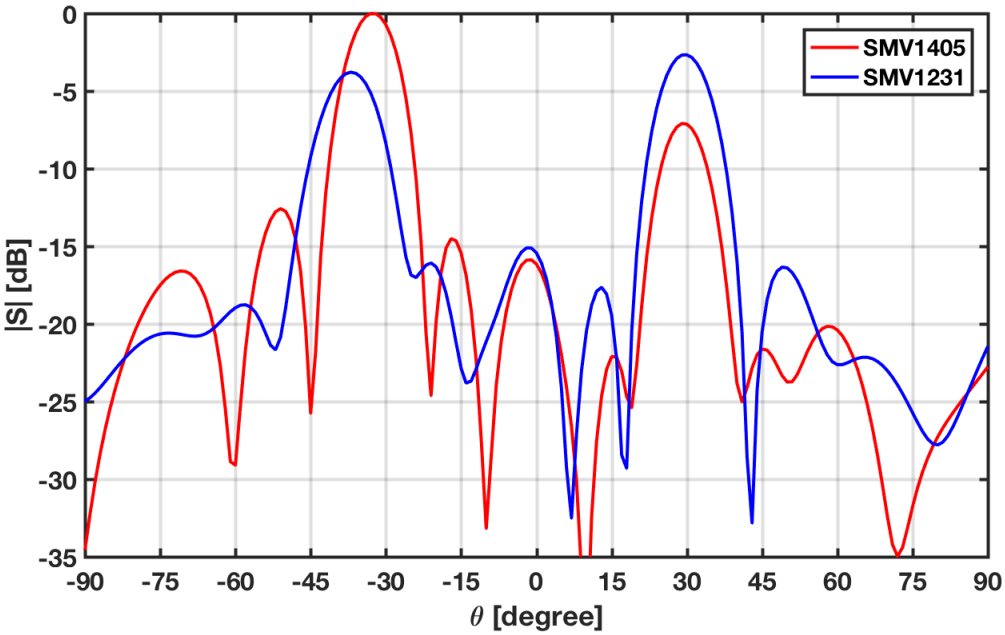

Figure 10 Radiation pattern for the same finite sample whose varactor is respectively modeled by SMV 1405 and SMV 1231 at their own resonant frequencies for the same bias capacitance *C = 1* pF. The one modeled by SMV 1405 has higher diffraction magnitude (peak at -33°) and lower reflection magnitude (peak at -30°) than the one by SMV 1231. The two patterns are normalized by the maximum of the diffraction for the one modeled by SMV 1405.

Part 2

Other Designs for Tunable Metasurface Grating

2.1 Design Goals

The final goal for the new designs is to improve the magnitude of the blazing. To achieve this, as our previous discussions, there are several features for the new designs, that is, be able to test if the varactor works well after soldering, have lower loss, and use less varactors if possible. Several designs are simulated and analyzed as following.

2.2 Tunable Patch with Three Bias Lines for Each Column

This design basically maintains the features of the previous one, but the bias system is different as the one shown before. The top view of unit cell for the structure is given in Figure 11 (a). It contains two split tunable patches. Each of the split patches shares exactly same dimensions as the previous design in Figure 2 (a). The bottom half part of one of the patches connects the top half part of the other patch by thin metal bias line. Thus the DC bias voltages can be applied on the bias lines as shown in Figure 11 (a). With this design, the varactors can be divided into two groups instead of one single group on each column, which will be helpful while testing them.

However, the simulation results, as shown in Figure 11 (b), indicate narrow band resonance and very low magnitudes of diffraction field for unit cell. In order to further explore if the resonant points in Figure 11 (b) are the desired resonant modes which will radiate and contribute to the diffraction field, we also simulate the field distribution at the resonant points and big difference is found by comparing them with the one in Figure 2 (b).

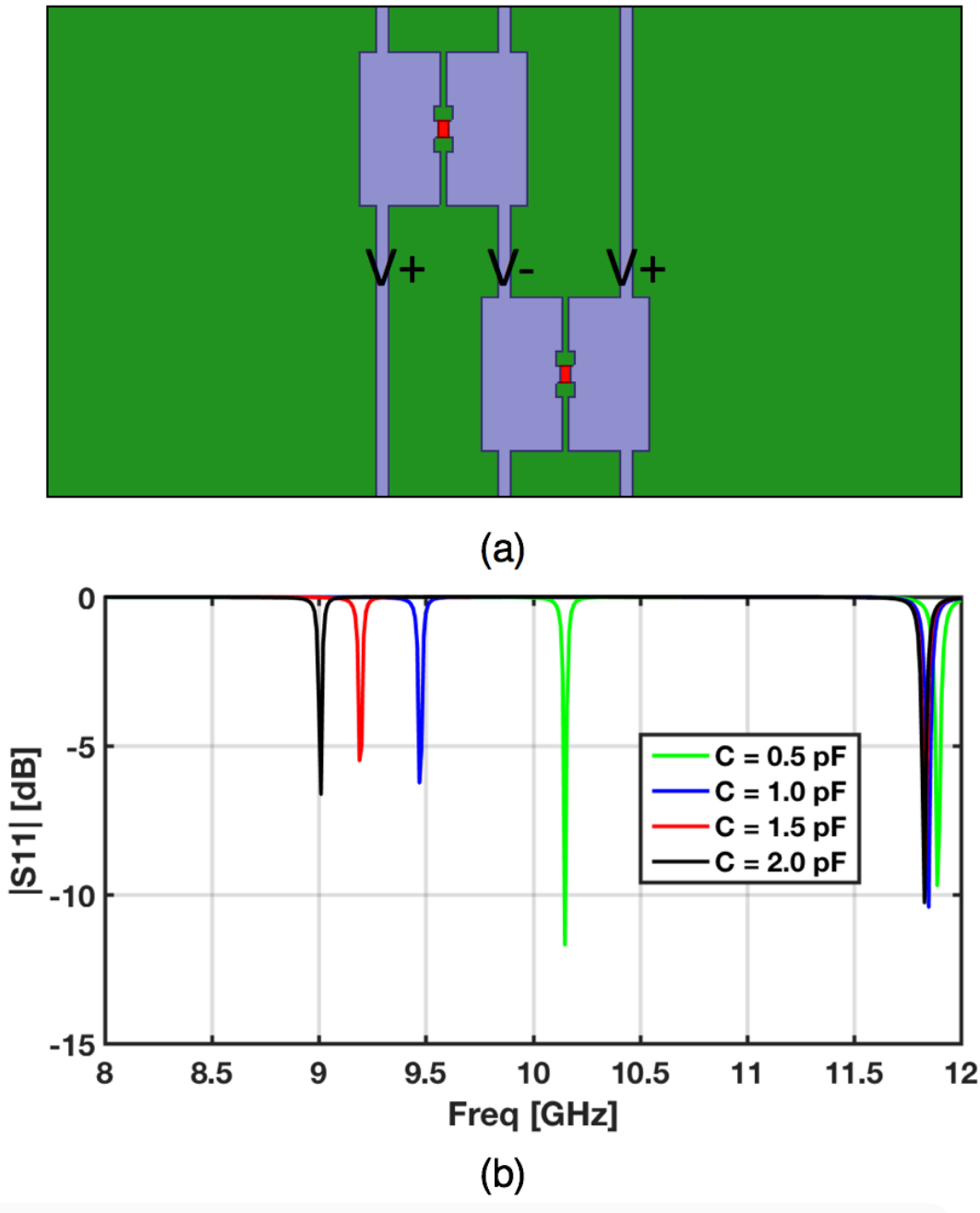

Figure 11 (a) Top view of unit cell for the three bias lines design. 'V+' and 'V-' represent the DC bias voltages. (b) Simulated magnitude of specular (*m = 0*) waves as a function of frequency at four different capacitances of the structure.

In conclusion for this design, the resonant mode is disturbed which means the design will possibly not even work as we expect, reflecting the incoming wave back. Meanwhile, since there are still half of the varactors are parallel-connected on each column, it is still impossible to test each of them after soldering. So it will possibly suffer from the non-uniform distribution

of the varactors as the previous design in Part 1.

2.3 Tunable Patch with Bias Via

In order to test each of the varactor, we come up with two designs with via to replacing one of the bias line in the original design. The diameter of the via is chosen to be 0.8 mm. It connects the top metallic layer and the bottom ground, so that the bias can be applied from the ground plane.

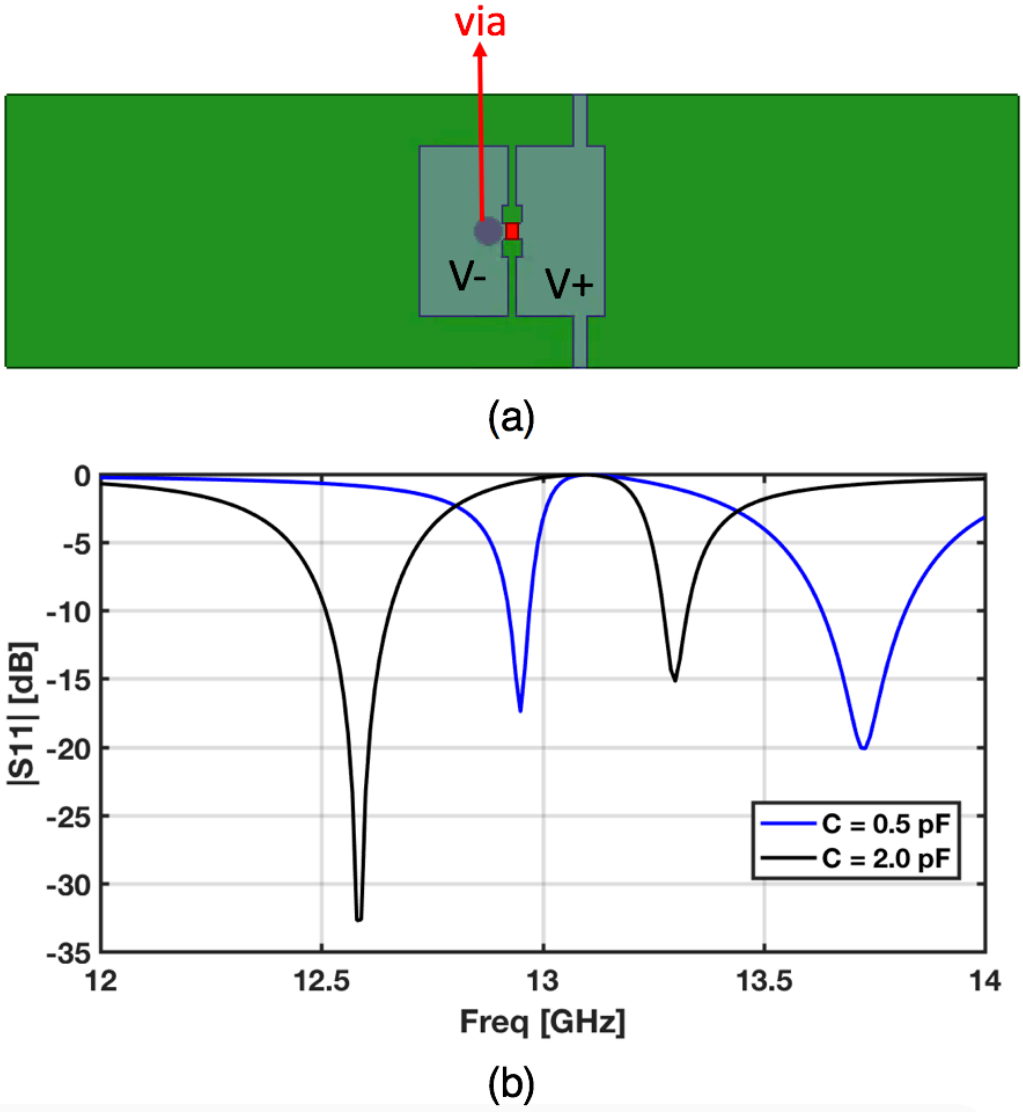

Figure 12 (a) Top view of unit cell for the design using only one via per unit cell. 'V+' and 'V-' represent the DC bias voltages. (b) Simulated magnitude of specular (*m = 0*) waves as a function of frequency at two different capacitances of the structure.

The unit cell for the design using one via is built and simulated as shown in Figure 12. The grey circle in Figure 12 (a) is the via. But the simulated S11 shows that the resonant frequency is much higher than the previous design and the resonant mode is still not the desired one which has been proved by the electric field profile at the resonant frequencies. Beside the position of via near the center of the patch, several other positions are also tested but the results are all not very convincing.

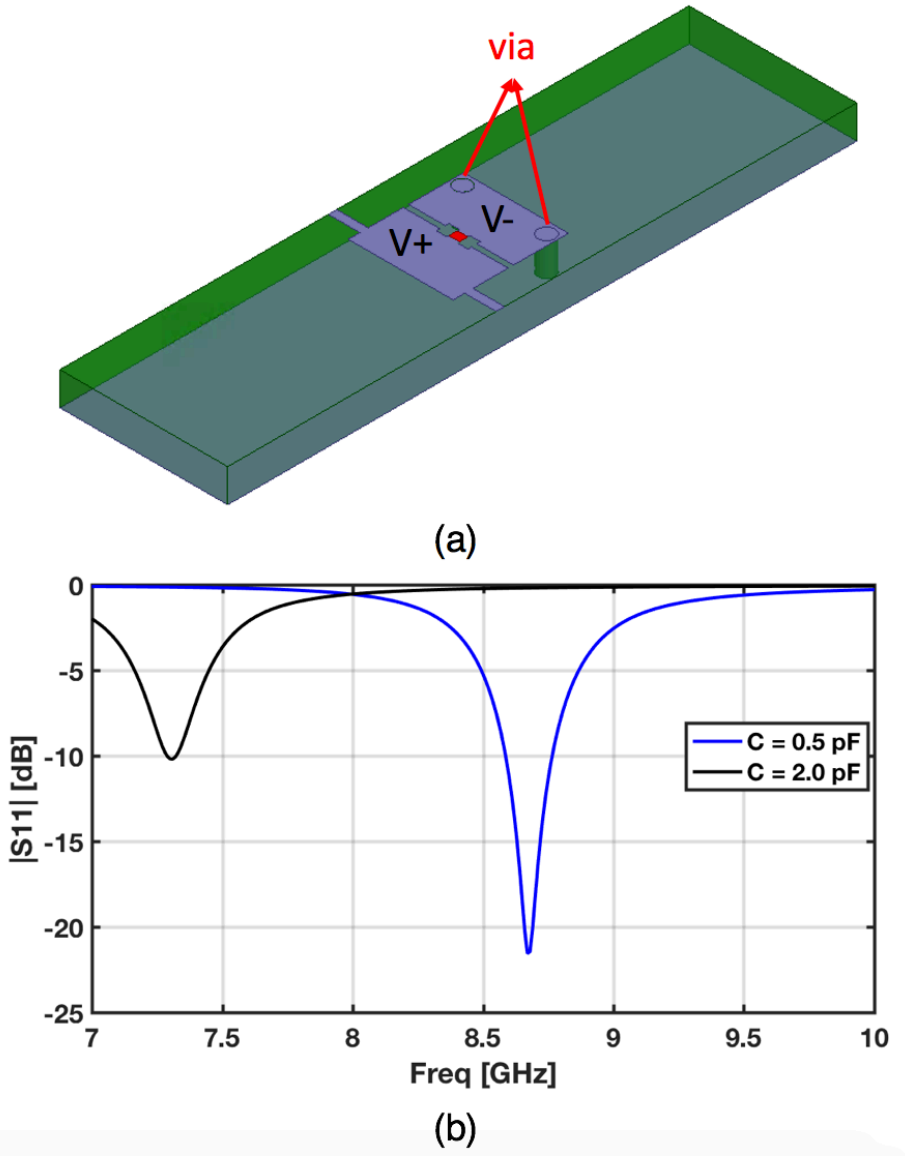

Figure 13 (a) Top view of unit cell for the design using two via per unit cell. 'V+' and 'V-' represent the DC bias voltages. (b) Simulated magnitude of specular (*m = 0*) waves as a function of frequency at two different capacitances of the structure.

The unit cell using two via is given in Figure 13 (a) and the simulated S11 for the structure is given in Figure 13 (b). The design using two via doesn't solve the previous problem, that is, the via helps the bias but also changes the resonant mode. This is because the inspired current on the patch will flow through the via to the ground and thus the design will not support the desired radiation mode.

In conclusion of the design with via, the resonant mode is disturbed similarly as the design in the previous section. Since this design also shares similar resonant structure as the previous designs, the total number of the varactor is still very large. In addition, we are still not able to test each of the varactor by this design, since for each column all the varactors are still parallel-connected. The only difference for this design is that the ground is used as bias instead of the bias lines connecting all the patches.

So the goal for the new design is to: 1) keep the same resonant mode; 2) respectively bias each of the varactor so that we are able to test each of them after soldering; 3) reduce the total number of the varactor.

2.4 Ground-Slotted Tunable Strip

Inspired by reconfigurable ground-slotted patch antenna [19], we decide to cut the slot on the ground and load with varactor. Meanwhile, the main resonator remains simple strip structure, same as the one used in [4, 5]. Its principle is depicted in Figure 14. The basic idea is to control the resonant frequencies with DC bias, same as the previous design.

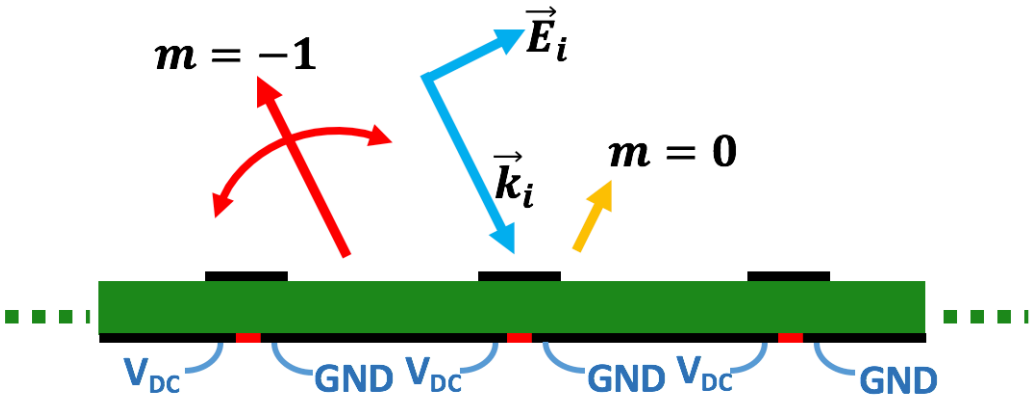

Figure 14 Ground-slotted electronically-tunable resonant blazed grating with DC-bias SMVs

The unit cell of the proposed tunable blazing structure is presented in Figure 15. The same period of the structure '*d*' as well as the grounded substrate Rogers RT5880 is used, same as the previous design. In order to reduce the total number of varactors that will be used for final sample fabrication, we extend the length of the unit cell '*l*' as 25 mm. This length of the unit cell is determined to balance the strong blazing behavior with the minimum number of the varactors for the whole structure. Note that later simulation results prove that there is no grating lobe showing up even though the length of the unit cell is larger than the half wavelength of the operating range. The main resonator is a 7-mm wide single strip on the top of the substrate, whose resonant behavior and operating principles have been well explored in [5]. It has to be mentioned that several designs associated with the idea for the ground slot have been built and tested in the simulation. The one shown in Figure 15 is the final version of the design that satisfied the all the requirements, and in the meantime it maintains the desired resonant mode and shows the strongest blazing performance as we expected.

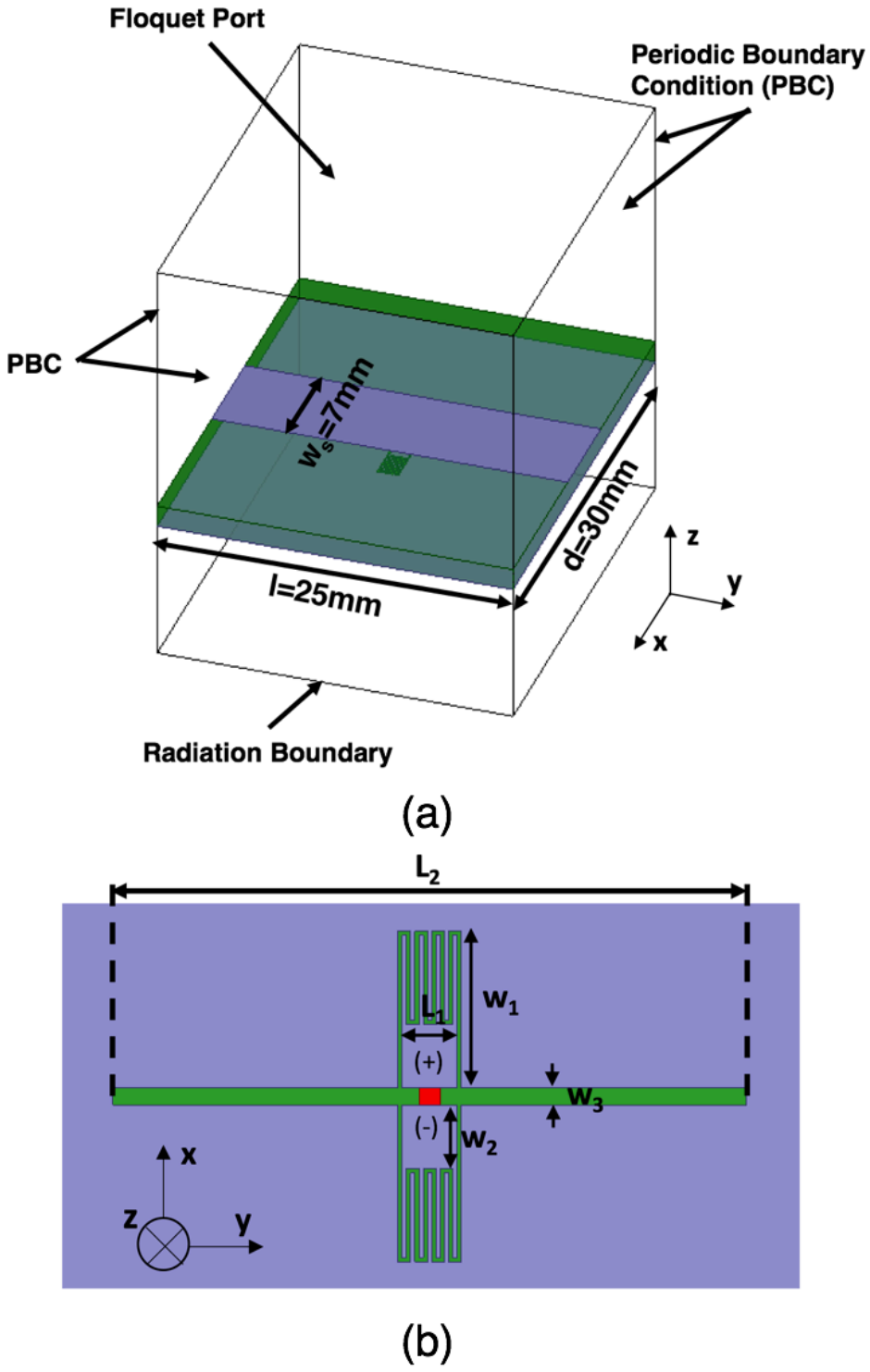

Figure 15 Geometry of the finite sample for the design from (a) top view and (b) bottom view. (c) Simulated scattering (in dB) of a finite sample at resonant frequencies with θ_i = -30°. The patterns are normalized by max. reflection of a same size PEC at f = 10.8 GHz (black dash line).

The 0.4-mm slot is cut at the ground right beneath the center of the strip. In order to be able to test each of the varactor after the soldering, the general idea is to design separate bias

patches for each varactor. Thus besides the main slot, additional cuts are needed for bias. These will bring in undesired parasitic effects which may destroy the performance. Constant capacitors are used to connect the additional cuts typically. Here we design two symmetric interdigital capacitors as shown in Figure 15 (b), instead of semiconductor capacitors, which will avoid additional loss. The ground slot has the dimensions of $L_1 = 1.3$ mm, $L_2 = 15$ mm, $w_1 = 3.7$ mm, $w_2 = 1.5$ mm, $w_3 = 0.4$ mm. The slots for the interdigital capacitors are 0.1 mm wide. Since the interdigital capacitors create DC block between the bias patches and the ground, we are able to test each of the varactor after soldering respectively. Meanwhile, bias lines can be attached to the bias patches to supply DC bias. The simulation results clearly show the tunability of this design, as in Figure 16.

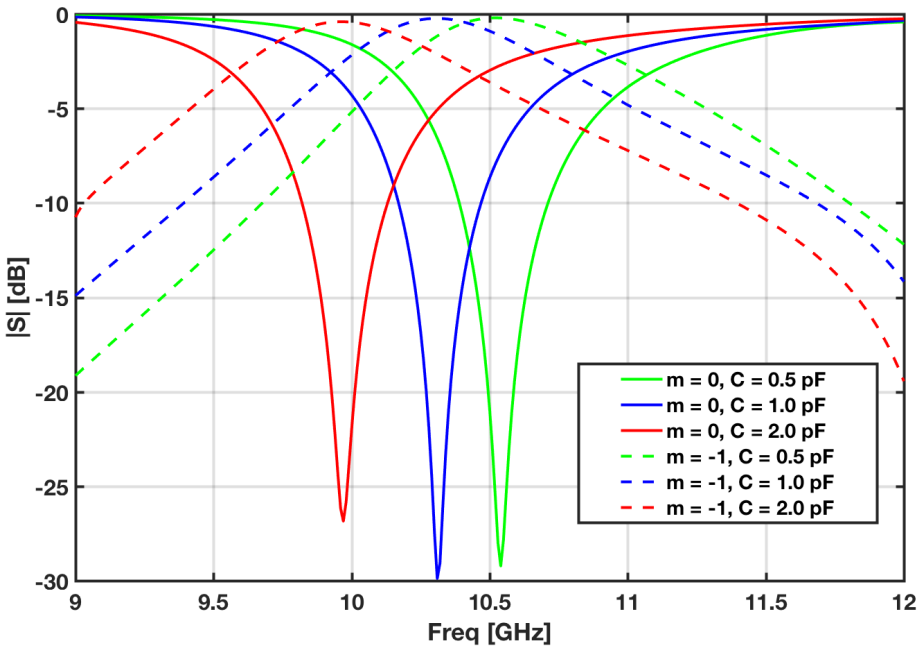

Figure 16 Simulated magnitude of specular (m = 0) and m = –1 waves as a function of frequency at three different capacitances of the new structure.

To further verify the tunability of this design, a finite sample is built and simulated as shown in Figure 17. The sample contains 6 by 5 unit cells in total as shown in Figure 17 (a)

and (b). The simulated scattering patterns are given in Figure 17 (c). As the capacitance is tuned from 0.5 to 2 pF, the resonant frequency shifts from 10.8 GHz to 9.8 GHz and the angle of the maximum diffraction scans from 25° to 31°.

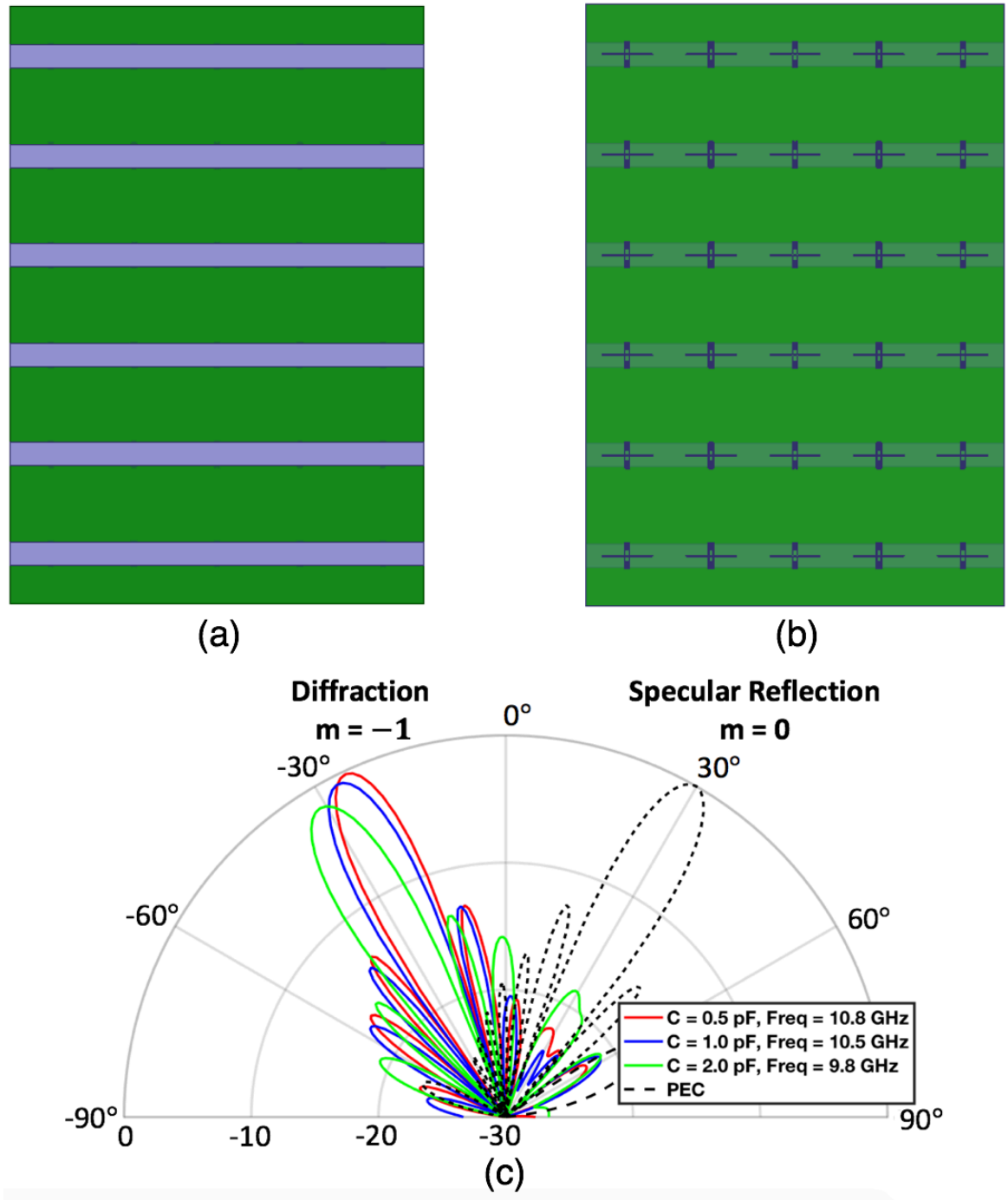

Figure 17 Geometry of the finite sample for the design from (a) top view and (b) bottom view. (c) Simulated scattering (in dB) of a finite sample at resonant frequencies with θ_i = -30°. The patterns are normalized by max. reflection of a same size PEC at f = 10.8 GHz (black dash line).

The finite sample shows the tunability and strong blazing numerically. However, the model of the varactor used in the simulation is a simple capacitance without any loss or package inductance. Thus in order to better simulate the real situation, we need to characterize the varactor based on our own measurement. Due to the limited time, the next sections are all proposed for the future work.

2.5 Future Work

In this section, future plans are listed in order to make sure a better measurement result for the ground-slotted structure. The following steps are based on what we have achieved so far and they may require further modifications to better match experimental results.

2.5.1 Varactor Characterization

In order to fully mimic the performance of the varactor in HFSS simulator, we need to re-characterize the varactor. Even though the vendor has given an equivalent circuit model for the varactor, it might not be accurate enough to be directly applied in the simulator. This inaccurate model of varactor is one of the possible reasons that causes the difference between the measurement result and the simulation results for the previous design as we have discussed in Part 1.

Our plan is to characterize the varactor based on the measurement results. The standard way to measure the circuit itself and eliminate the undesired error caused by transition parasitics is thru-reflect-line (TRL) calibration [20]. The basic idea is to measure three sets of data, namely ‘thru’, ‘reflect’, and ‘line’, as reference, and use these reference data to calibrate the target measurement results. This method will be used to first acquire the accurate S

parameter response of the varactor on the same board that we will use for grating sample fabrication within the desired frequency band.

With the measured response, we plan to optimize the Lumped RLC Boundary in Ansys HFSS to mimic the real response as accurately as possible. It has been reported that the lumped port can be used in full-wave solvers along with the measured response to fully characterize the lumped component [21]. However, this method can only be applied to simulate the S parameters response, instead of the far field distribution as we need for our design. So the best way is to use the Lumped RLC Boundary to build the model and optimize it to match the measured response.

2.5.2 Iteration to Refine the Design

Once we have the accurate model to characterize the varactor, then we can use the model to refine the design in order to get a stronger blazing and wider tunable band. The procedures for the refine the parameters can be iterated in order to get the best results.

Then the final step will be fabrication and measurement. The fabricated new design also has the added benefit that we can test each of the varactor to check if they are well-connected and well-function. Besides that, we are going to use RF choke for each bias line to block the RF signal.

CONCLUSION

An electronically tunable resonant blazed grating is demonstrated in simulations and experiment at X-band in Part 1, without having any moving parts. Varactor is used in the design to achieve the electronical tunability. And the possible reasons for the low blazing in the measurement have been discussed at the end of Part 1. Based on the discussion, we propose several designs in Part 2 to overcome the problems left in the previous design. The tunability and strong blazing performance of the ground-slotted design has been numerically proved. Future work to refine the design is also proposed in the end, following which we will have a promised measurement result for the ground-slotted design.

The presented concept can be an enabling element in a variety of applications. For example, in Littrow cavities without the need to rotate the blazed grating itself, to tune the Littrow cavity frequency. The idea presented can be used at mm-waves and THz, with same or similar geometries and can be extended for both polarizations.

REFERENCE

[1] T. Itoh and R. Mittra, “An analytical study of the echelette grating with application to open resonators,” IEEE Trans. Microw. Theory Tech., vol. 17, pp. 319-327, Jun. 1969

[2] A. Hessel, J. Schmoys, and D. Y. Tseng, “Bragg-angle blazing of diffraction gratings,” J. Opt. Soc. Am., vol. 65, no. 4, pp. 380-384, 1975.

[3] X. Li, M. Memarian, K. Dhwaj, T. Itoh, “Blazed metasurface gratings: Planar equivalent of sawtooth gratings,” in IEEE Int. Microw. Symp., San Francisco, CA, USA, May 2016.

[4] M. Memarian, X. Li, T. Itoh, “Resonant blazed metasurface gratings,” European Microwave Conference, pp. 297-300, Oct. 2016.

[5] M. Memarian, X. Li, Y. Morimoto, T. Itoh, “Wide-band/angle Blazed Surfaces using Multiple Coupled Blazing Resonances”, accepted in Scientific Reports, Jan 2017.

[6] Masud, Muhammad Mubeen, et al. "A compact dual-band emi metasurface shield with an actively tunable polarized lower band." IEEE Transactions on Electromagnetic Compatibility 54.5 (2012): 1182-1185.

[7] Martinez, Idellyse, et al. "Ultra-thin reconfigurable electromagnetic metasurface absorbers." Antennas and Propagation (EuCAP), 2013 7th European Conference on. IEEE, 2013.

[8] Debogovic, Tomislav, and Julien Perruisseau-Carrier. "Low loss MEMS-reconfigurable 1-bit reflectarray cell with dual-linear polarization." IEEE Transactions on Antennas and Propagation 62.10 (2014): 5055-5060.

[9] Feng, Yijun, et al. "Dynamically controlling electromagnetic wave with tunable

metasurfaces." 2015 International Symposium on Antennas and Propagation (ISAP). IEEE, 2015.

[10] Pavone, Santi C., et al. "A novel approach to low profile scanning antenna design using reconfigurable metasurfaces." 2014 International Radar Conference. IEEE, 2014.

[11] Su, Xiaoqiang, et al. "Broadband terahertz transparency in a switchable metasurface." IEEE Photonics Journal 7.1 (2015): 1-8.

[12] Mavridou, M., and A. P. Feresidis. "A new class of tunable multi-layer meta-surfaces." Advanced Electromagnetic Materials in Microwaves and Optics (METAMATERIALS), 2014 8th International Congress on. IEEE, 2014.

[13] Gordon, Joshua A., et al. "Fluid interactions with metafilms/metasurfaces for tuning, sensing, and microwave-assisted chemical processes." Physical Review B 83.20 (2011): 205130.

[14] Zhu, W. M., et al. "Tunable flat lens based on microfluidic reconfigurable metasurface." 2015 Transducers-2015 18th International Conference on Solid-State Sensors, Actuators and Microsystems (TRANSDUCERS). IEEE, 2015.

[15] Kamali, Seyedeh Mahsa, et al. "Tunable dielectric metasurfaces using elastic substrates." CLEO: Science and Innovations. Optical Society of America, 2016.

[16] X. Li, C. Antoine, D. Lee, J. Wang and O. Solgaard, "Tunable Blazed Gratings", J. Microelectromech. Syst., vol. 15, no. 3, pp. 597-604, 2006.

[17] Y. Fan, and Y. Rahmat-Samii, “Patch antennas with switchable slots (PASS) in wireless communications: Concepts, designs, and applications”, IEEE Antennas Propag. Mag., vol. 47,

no. 2, pp. 13–29, Apr. 2005.

[18] Hsiao, Y. T., Lin, Y. Y., Lu, Y. C. and Chou, H. T., "Applications of time-gating method to improve the measurement accuracy of antenna radiation inside an anechoic chamber," IEEE Antennas and Propagation Society International Symposium, vol. 3, pp. 794-797, Jun. 2003.

[19] Byun, Seung-Bok, et al. "Reconfigurable ground-slotted patch antenna using PIN diode switching." ETRI journal 29.6 (2007): 832-834.

[20] Engen, Glenn F., and Cletus A. Hoer. "Thru-reflect-line: An improved technique for calibrating the dual six-port automatic network analyzer." IEEE transactions on microwave theory and techniques 27.12 (1979): 987-993.

[21] Yousefbeiki, Mohsen, and Julien Perruisseau-Carrier. "A practical technique for accurately modeling reconfigurable lumped components in commercial full-wave solvers [EurAAP corner]." IEEE Antennas and Propagation Magazine 54.5 (2012): 298-303.